A New Unstructured-Mesh Method for Flow Prediction in Internal Combustion Engines

B.Adamson, A.D.Gosman, C.J.Marooney, B.Nasseri and T.Theodoropoulos

Mechanical Engineering Department
Imperial College
Exhibition Road
London SW7 2BX
U.K.

ABSTRACT

The finite-volume method (FVM) for discretization in computational fluid dynamics (CFD) has the advantage that, unlike the finite difference approach, where derivatives are discretized, the FVM always works in terms of discretization of physical quantities such as convective and diffusive fluxes between control volumes. This permits the method to be extended to unstructured meshes where inter-cell differences cannot be defined in terms of discretized curvilinear derivatives, but the physical quantities can still be defined. The use of such unstructured meshes permits flow boundary geometries to be meshed for a variety of practical industrial cases, without causing any problems due to large mesh distortion.

This paper presents the implementation of such a method in a fully implicit computer code, SPEED, which allows fast and efficient 3D-CFD calculations in realistic geometries for reciprocating engine combustion chambers. SPEED uses a mixed Eulerian/Lagrangian calculation method for transport of continuous fields in a mesh moving in response to boundary motion, with the option of adding and removing mesh cells. The unstructured mesh presumes a single type of mesh connectivity, quadrilateral-sided hexahedra with six nearest neighbours, which allows local mesh refinement, with the potential for insertion of refinement to give flow-adaptive meshing. The mesh is in general non-orthogonal, and the pressure-velocity coupling is made through a non-orthogonal extension of the EPISO algorithm, modified to accomodate the unstructured mesh.

SPEED supports airflow and homogeneous combustion calculations, and also has a Diesel spray module; it is currently under development to include autoignition, inhomogenous combustion and soot and NO_x formation to give full IC engine performance prediction. The performance of the code is here evaluated with reference to the airflow calculation mode by presenting predictions of flows in a test engine with three geometries: (a) simple disc chamber; (b) re-entrant lipped bowl; (c) square bowl. Comparisons are made with experimental LDV measurements.

1. INTRODUCTION

The role of computational fluid dynamics (CFD) in the prediction of complex flow systems has been enhanced in recent years by two factors. On the one hand, the need has grown for accurate predictions of three-dimensional flows in plant and engine simulations, due to the drive towards increased efficiency, economy and safety standards. At the same time, the technology to make such computations fast and affordable has also reached the point at which such simulations are now feasible within normal industrial design timescales. While the mathematical development needed for such computations has already been embodied, for the internal combustion engine, in codes such as KIVA [1] and EPISO [2], their discretized space has always been a distorted rectangular mesh. This sets a limit to the efficiency of such meshes to capture the flow in domains which may be multiply-connected and which have highly re-entrant boundaries.

To remedy this, the SPEED code [3] has been developed at Imperial College, to implement the EPISO code algorithm on an unstructured mesh of the finite-element type, but using the finite-volume method (FVM). In the next section we show how this method is derived from the transport equations, and how the discretized form maps back into the differential form. This method has permitted the meshing of Diesel engine geometries in a way that minimizes the departure from orthogonality, and allows the mesh to approach uniform density despite the need to fit simultaneously such engine structures as open valves and bowl-in-piston geometries. In section 3, we describe, as an example of this, calculations of the induction and compression flow in a motored engine, for which measurements had already been made at Imperial College [5]. The results for this are presented in section 4.

The unstructured nature of the mesh also permits the (as yet unrealized) possibility of dynamic rezoning using local mesh insertion. Section 5 offers some conclusions on the potential of the present method for extending CFD.

2. METHODOLOGY

(a). Discretization

We seek to solve the transport equation for a typical conserved scalar ψ

$$\frac{\partial \rho\psi}{\partial t} = -\nabla\cdot(\rho\mathbf{U}\psi - \Gamma\nabla\psi) + Q + q\psi \qquad (1)$$

where the terms with Q,q are a linearized form of the source terms. In the implicit FVM, the equation is first integrated over a mesh cell C (domain Ω), after which the time-derivative is forward-differenced and the integrals of divergences are replaced by surface integrals over the divergence operand, after Gauss' theorem. This yields (superscript zero denotes old-time values)

$$\frac{1}{\Delta t}\int_{\Omega} dV(\rho\psi - \rho^{\circ}\psi^{\circ}) = -\sum_{f=1}^{N_F(C)}\int_{\partial\Omega_f} d\mathbf{S}\cdot(\rho\mathbf{U}\psi - \Gamma\nabla\psi) + \int_{\Omega} dV(Q + q\psi) \qquad (2)$$

which is still exact. It is assumed that cell C has $N_F(C)$ faces: the surface integral is divided into integrals over each face f (domain $\partial\Omega_f$). In general, face f will have $N_N(C,f)$ neighbours. If we make the approximations that within the cell and over the interface between two cells the transported quantity ψ is constant, then Eq.(2) yields the discrete form

$$\frac{V_C(\rho_C\psi_C - \rho_C^{\circ}\psi_C^{\circ})}{\Delta t} = -\sum_{f=1}^{N_F(C)}\mathbf{S}_f\cdot(\rho_f\mathbf{U}_f\psi_f - \Gamma_f\mathbf{G}(\psi)_f) + V_C(Q_C + q_C\psi_C) \qquad (3)$$

(where $\mathbf{G}$ is the discrete equivalent of ∇) and the cell-boundary quantities ψ_f are then evaluated from the cell-centre quantities ψ_C by conventional differencing practices. In the present version of the SPEED code, central differencing is used for all variables other than the dependent convected variable, where hybrid upwind differencing is assumed, although this is not a restriction on the method. The extension to moving meshes is also straightforward.

Gradients are also treated by Gauss' theorem, yielding an appropriate expression for the pressure force term. The intensive (i.e. without volume integration) gradient arising in the diffusion term is also modelled in this way, but the cell over which it is evaluated is the prism of translation produced by sliding the face area from one cell centre to the neighbour centre: this yields the operator $\mathbf{G}$. This staggered cell has volume V_f with $N_f(C,f)$ faces of area $\mathbf{S}^f$. The finalised FVM transport equation is then

$$\frac{V_C\rho_C\psi_C - V_C^{\circ}\rho_C^{\circ}\psi_C^{\circ}}{\Delta t} = -\sum_{f=1}^{N_F(C)}\left(\rho_f\mathbf{U}_f\psi_f - \frac{\Gamma_f}{V_f}\sum_{l=1}^{N_f(C,f)}\mathbf{S}_l^f\psi_l^f\right)\cdot\mathbf{S}_f + V_C(Q_C + q_C\psi_C) \qquad (4)$$

The staggered mesh generated by the face-cell construction is not a computable mesh if the parent mesh is unstructured, since the face cells do not connect but overlap. The preferred choice of variable location is thus the cell-centre for all variables. Pressure chequerboarding is avoided in the conventional manner, using, as auxiliary variable, the mass flux density, which, unlike the transported quantities, can be effectively located on the staggered mesh.

(b). Choice of mesh

SPEED engine calculations are performed on geometries with $N_N(C,f)=1$ for all C,f to give a uniform local topology yielding a single code strategy for the whole mesh, and $N_f(C)=6$ (with quadrilateral interfaces). The strategies with $N_N>1$ are more appropriate to mesh refinement (and multigrid methods) on a rectangular mesh (but also for slipping meshes in rotor systems), whereas the unstructured mesh with the uniform local topology permits local refinement. The hexahedral cells are chosen to permit addition and removal of whole cell layers, to track piston and valve motion in engine calculations.

In the example calculation chosen for the present study, the mesh used to realise the bowl-in-piston DI Diesel geometry utilizes the local refinement option in the swirl plane to realize an approximation to uniform mesh density, as shown in fig. 1. This procedure also distributes non-orthogonality such that the non-orthogonal skew between cells can be in either sense, compared with the need for a rectangular mesh to have the same skew in all cells in a given region, and so yields the possibility of minimizing the non-orthogonality. The mesh is generated with the PATRAN CAD package, which imposes some limitations on achieving a completely unstructured mesh, and it is conjectured that a fully random tiling of the plane would go further to achieving this distribution of density and non-orthogonality. The mesh is regular in the direction of piston motion (fig. 2c) to allow layer addition and removal, although this is done for convenience outside the squish region and need not apply in the piston bowl.

3. CALCULATION

The above-described calculation procedure has been used to calculate motored flow in an experimental configuration consisting of a single-cylinder test engine, with inlet swirl imparted through a helical inlet port from a FIAT X8/65E1 engine. A re-entrant bowl-in-piston geometry was employed, as seen in the calculated flow fields of figure 3. LDV measurements have been made for this configuration[5] and form the basis for the comparisons in the next section.

Inlet flow conditions are imposed at the valve curtain;

the port was not modelled in the present application although it is not a restriction of the method. The inlet velocities were also measured for this case during the engine cycle by LDV[5], but the azimuthal resolution is coarse (3 points) and is here supplemented by interpolation on the basis of other studies[6]. Wall boundary conditions are imposed via wall functions. The flow calculation is fully implicit compressible flow, using the PISO[4] pressure-velocity coupling. The turbulent contribution to the ensemble-averaged equations is realized by the k-ε model.

Calculations were performed on an Apollo DN-10000, with the peak mesh size (140K cells) necessitating the migration to a virtual-memory machine. Previous validation work indicated that this mesh size was required for full resolution of the flow, and points to the need to go to higher-order differencing schemes.

4. RESULTS

The LDV measurements were made at the engine crank angles 57°, 108°, BDC, IVC(245°), 320°, 340° and TDC compression, along one or two axes perpendicular to the piston motion in the symmetry plane of the engine geometry. For reasons of space, it is not possible to give details of comparisons at all these angles, and we confine ourselves to 57°, 108° and 340°, referring parenthetically to the others where appropriate. The calculated flow fields for 57°, 108° and 180° are shown in figs. 2 (axial plane) and 3 (diametral plane), and for 340° in fig. 4 (axial plane only).

The interaction of swirl and squish for this off-centre valve plus centred bowl geometry is more complex than might be expected from previous results obtained with codes whose use of axisymmetric meshes meant so that either the off-centred valve or the centred bowl, but not both, could be included. In both measurement and calculation, an induction jet produces recirculation regions above and below it, and also in the piston bowl; the port-generated swirl causes swirl motion in the chamber, which persists with some decay through to TDC compression; compression causes squish vortices to form in the bowl. Solid-body swirl is not established until well after BDC, with a substantial reverse-circulation region anticlockwise of the valve, and around BDC a vortex forms in the bowl throat; precursors of these features are observed earlier in the stroke. In some cases, these features, which would not be seen in axisymmetric calculations, are not represented in the geometrical symmetry plane, and so are not seen by the measurements, which were confined to that plane.

Turning now to the comparison between measurement and calculation, fig. 5 shows the comparisons at 57° and 108°ATDC. Two meshes were used: both had variable sizes due to the addition and removal of layers during piston and valve motion, so that the relevant standard of comparison is their peak sizes, 30 000 and 140 000 respectively. A major area of disagreement for the swirl flow in the coarser mesh is the recirculation vortex on the left of fig. 2a: this is inadequately resolved with this mesh size, and further refinement yields good agreement. The axial flow trends are good at both resolutions, but the numerical diffusion is significantly reduced at the higher resolution. The principal discrepancy is the overall swirl profile. This is not reduced at the higher resolution, which indicates that mesh independence is being reached, and suggests either that the extrapolation of the coarsely measured inlet flow distribution is not correct, or that the eddy-viscosity level of turbulence modelling is not adequate. These trends continue in the comparison at 108°ATDC.

It is also important to note that comparison of calculation and measurement on a single line through the chamber gives limited indication of the accuracy of the three-dimensional nature of the calculated flow. Inspection of the calculated swirl field at 108°ATDC (fig. 3b) shows that the measurement (fig.5d) is more representative of the flow along a line rotated 10° anticlockwise. One expects that small uncertainties in the inlet swirl distribution will alter the positioning of flow features, but conserve their size and topology, as is observed here.

Agreement with measurement improves after IVC, as the discrepancies associated with the inflow data decay, and features associated with the squish generation of the bowl-in-piston geometry start to dominate. In the squish vortex pattern in the bowl at 340°ATDC (fig. 4, on the coarser 30 000 cell mesh, the finer-mesh results not yet being available), the assymetry is partly due to the bowl eccentricity, and partly due to the residual effects of the assymetric induction-created flowfield. Fig. 6 shows the axial and swirl flow comparisons. The swirl flow comparisons show the expected near-solid-body swirl pattern. The underprediction of the angular momentum is expected on a mesh of this density using conventional upwind differencing, and companion calculations of disc chamber flow in the same engine yield 90% of the measured swirl velocity at TDC compression, showing that the correct level of angular momentum should be obtainable with the finer mesh. The squish flow profile shows that while the correct pattern of flow is obtained, the amount of central upflow is underpredicted. This is thought to be due to the fact that the crevice volume is not modelled. This volume is large in optically-accessed engines as the piston rings are lowered to permit uninterrupted optical access to the bowl, and will be included in the finer mesh calculation.

Turbulence calculations at 108°ATDC (not displayed due to space limitations) give an average r.m.s. flow speed of 3.1 m s^{-1} for the finer mesh compared with a measured 5.2 m s^{-1}. This is an improvement on the coarser mesh value of 2.0 m s^{-1} but suggests that complete mesh independence is not achieved. Companion calculations of disc chamber flow in the same engine show, however, that at the finer mesh density good agreement with measurement is obtained at TDC of compression (the only measurement in that geometry.) As the predominant turbulence production mechanism in the disc chamber geometry is swirl decay, this suggests that the swirl uncertainties in this calculation may be contributing to the underprediction of turbulence.

5. CONCLUSIONS

The ability to use FVM on unstructured meshes provided in SPEED greatly increases the number of engine geometries for which detailed calculations can be performed, up to and including, in principle, the full geometry of *n* cylinders plus manifold connections (subject of course to computer size and speed.) Equally, it provides the possibility of combining this with local dynamic mesh refinement for efficient tracking of changes in flow conditions. The choice of uniform local

topologies has avoided the need for cumbersome interlocking pieces of specialized code in favour of a single and elegant treatment, which will be the desirable choice not only in terms of present code maintenance, but also of incorporation within developments in computing language and architecture.

In the present study, it is clear that the flows capable of being calculated with SPEED need careful visualization, not only in characterization through measurement, but also in graphical representation of computational results. The present method extends present meshing and graphics capabilities to their limits and indicates the need for further development in these fields. This will become more acute as the development of SPEED for full Diesel combustion within the IDEA program[3] multiplies not only the flow phenomena but also the number of interacting fields. It is anticipated that SPEED, due to its flexible architecture which permits the rapid inclusion of new models within an implicit framework, will be an important tool in this development.

ACKNOWLEDGEMENTS

Thanks are due to C. Vafidis for valuable discussions, and H. G. Weller for assistance with computing. The methodology embodied ion the SPEED code was developed with the financial assistance of the UK Science and Engineering Research Council, the Commission of the European Community, and the Joint Research Committee of Austin-Rover, Fiat, PSA, Renault, Volkswagen and Volvo.

REFERENCES

1. T D Butler, A A Amsden, P J O'Rourke aand J D Raamshaw: "KIVA: a comprehensive model for 2D and 3D engine simulations." SAE-850554, 1985

2. A D Gosman, Y-Y Tsui and A P Watkins: "Calculation of three-dimensional air motion in model engines." SAE-840229, 1984

3. A D Gosman and C J Marooney: "Development and validation of computer models of in-cylinder flow and combustion in Diesel and spark-ignition engines." C399/169, IMechE, Autotech '89, Birmingham England, 1989.

4. R I Issa: "Solution of the implicitly discretized fluid-flow equations by operator-splitting." J.Comp.Phys, 62, 40-65, 1986

5. C Vafidis, G Vorropoulos, J Whitelaw, and E Nino, "In-cylinder flowfield in a motored engine equipped with a helical port and with re-entrant ans square piston-bowl configurations", Imperial College, Department of Mechanical Engineering, Fluids Section Report FS/87/41, 1987

6. W Brandstatter, R J R Johns, and G Wigley, "Calculation of the flow produced by a tangential inlet port", in Int. Symp. on flows in internal combustion engines III (ASME, FED - vol 28), 1985

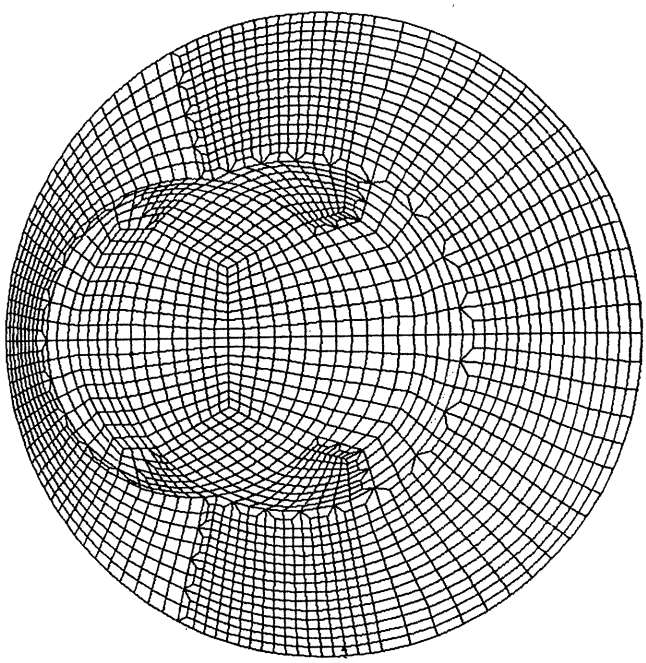

Fig. 1. Diametral plane of the PATRAN-generated unstructured mesh, showing the bowl and valve circles.

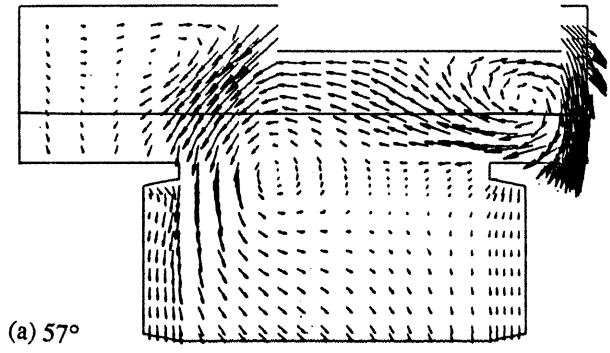

Fig. 2. Axial flow fields at (a) 57°, (b) 108°ATDC, (c) BDC.

The horizontal lines across the flowfields in figs. 2, 3 and 4 show the axes of the LDV measurements for the comparisons in fig. 5.

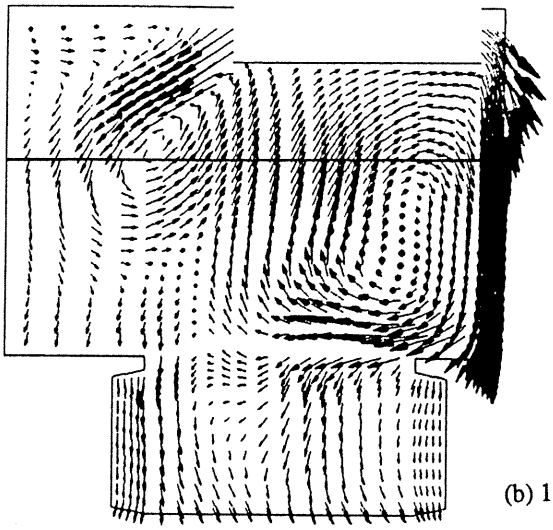

(b) 108°

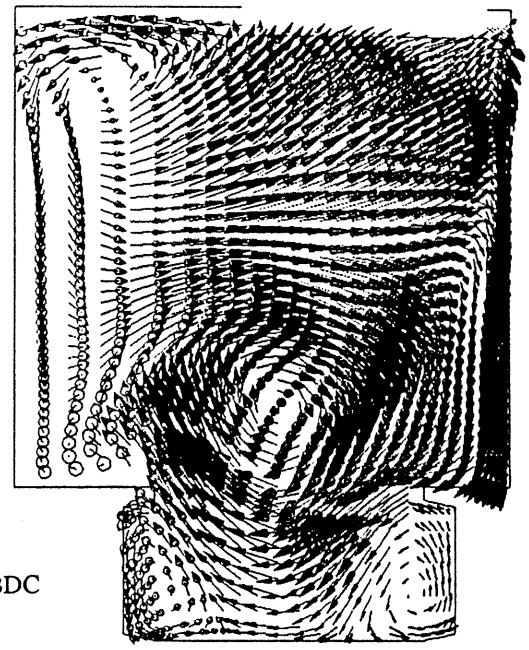

(c) BDC

Fig. 2. Axial flow fields at (b) 108°ATDC, (c) BDC.

Fig. 3. Swirl flow fields at (a) 57°, (b) 108°ATDC, (c) BDC elevation -15mm, (d) BDC elevation -35mm.

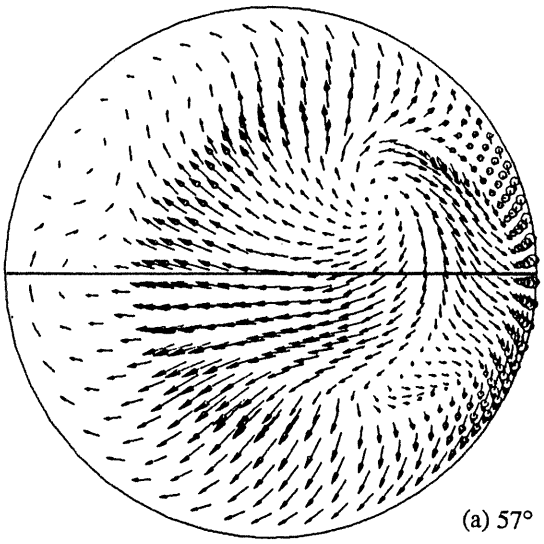

(a) 57°

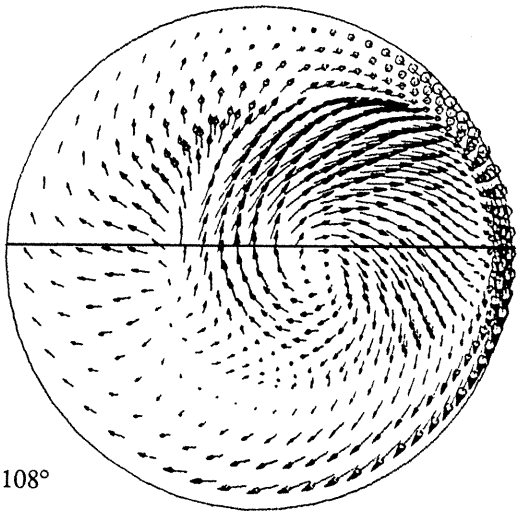

(b) 108°

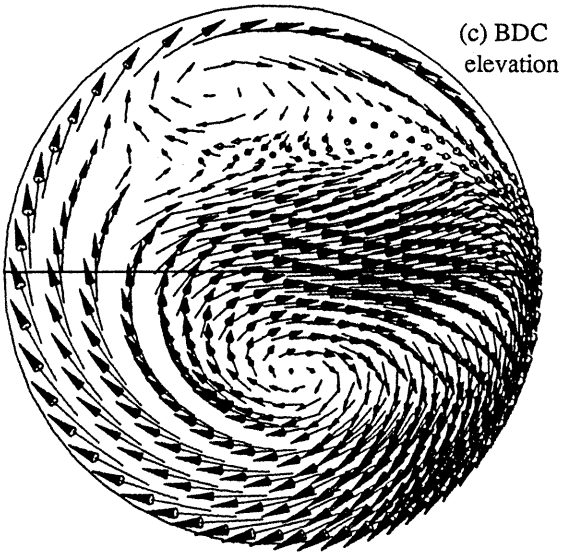

(c) BDC
elevation -15mm

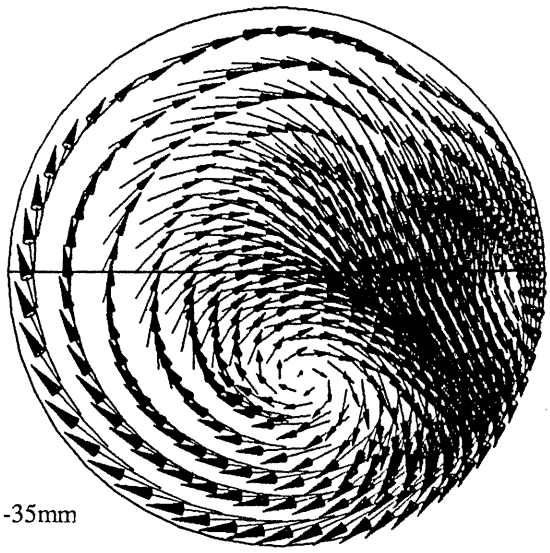

(d) BDC
elevation -35mm

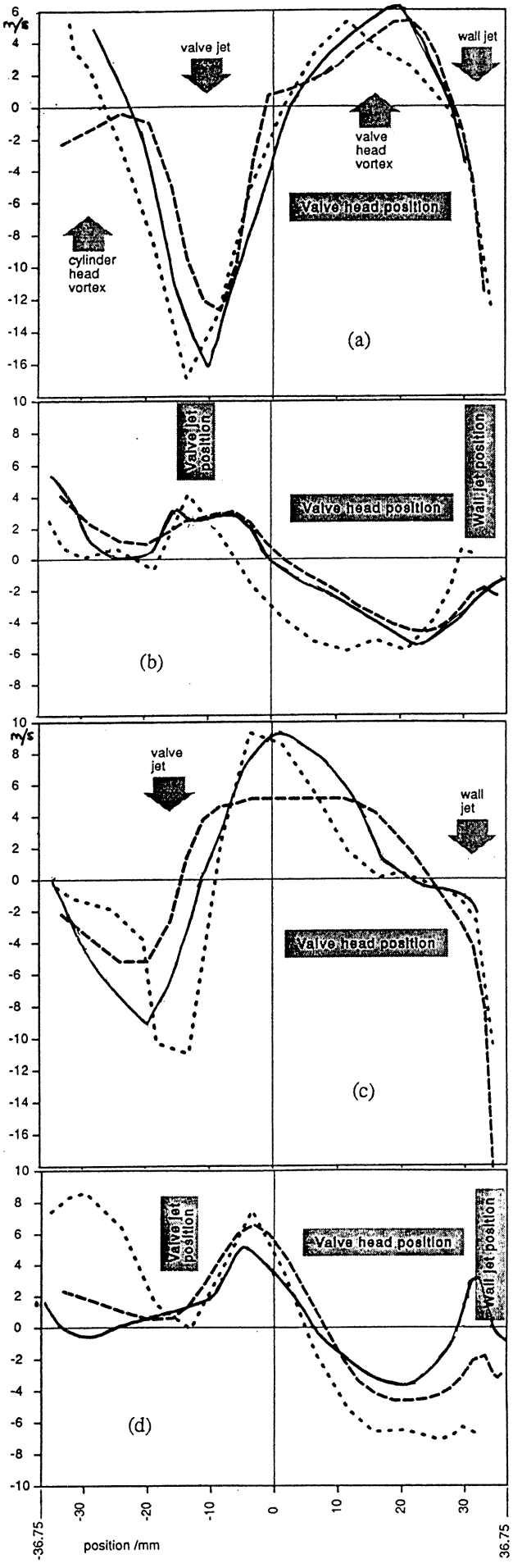

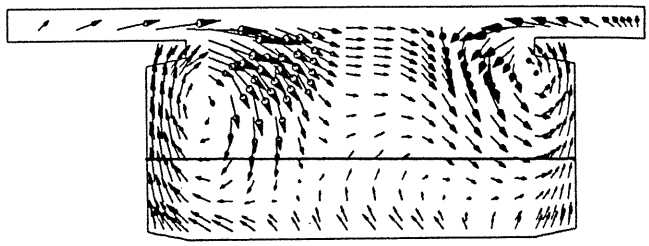

Fig. 4. Axial flow field 340°ATDC.

Fig. 5. Comparison between calculation and measurement, (a) axial flow 57°, (b) swirl flow 57°, (c) axial flow 108°, (d) swirl flow 108°.
..... = measurement, - - - - =coarse mesh,
——— = fine mesh

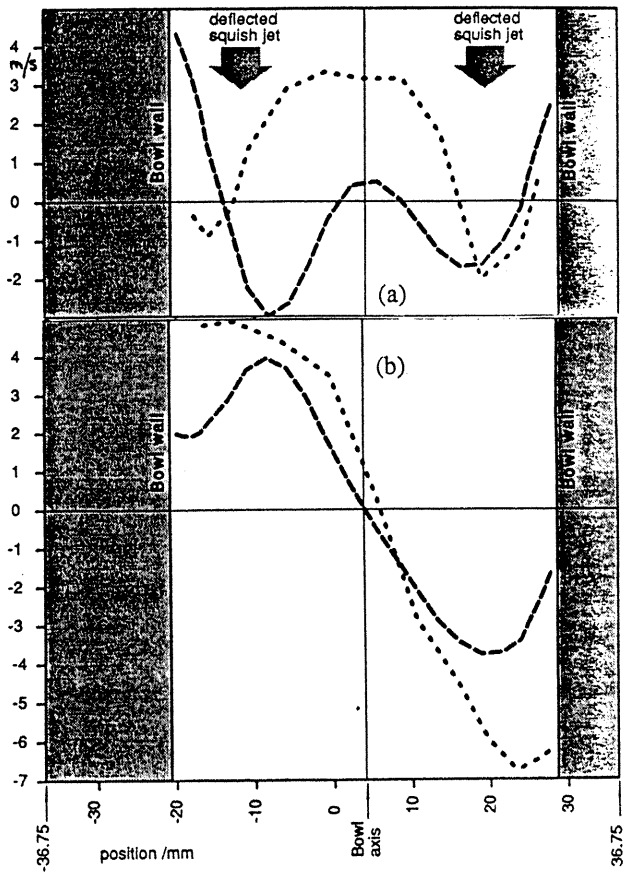

Fig. 6. Comparison between calculation and measurement, 340° ATDC: (a) axial flow, (b) swirl flow.
- - - - = measurement, ———— =coarse mesh